

Article

SUMOylation of α -tubulin is a novel modification regulating microtubule dynamics

Wenfeng Feng^{1,2,†}, Rong Liu^{1,†}, Xuan Xie¹, Lei Diao¹, Nannan Gao¹, Jinke Cheng³, Xu Zhang^{2,4,5}, Yong Li³, and Lan Bao^{1,5,*}

¹ State Key Laboratory of Cell Biology, CAS Center for Excellence in Molecular Cell Science/Shanghai Institute of Biochemistry and Cell Biology, University of Chinese Academy of Sciences, Chinese Academy of Sciences, Shanghai 200031, China

² Institute of Brain-Intelligence Technology, Zhangjiang Laboratory; Shanghai Research Center for Brain Science & Brain-Inspired Intelligence, Shanghai 201210, China

³ Discipline of Neuroscience and Department of Biochemistry, Collaborative Innovation Center for Brain Science, Shanghai Jiao Tong University School of Medicine, Shanghai 200025, China

⁴ Institute of Neuroscience and State Key Laboratory of Neuroscience, CAS Center for Excellence in Brain Science, Chinese Academy of Sciences, Shanghai 200031, China

⁵ School of Life Science and Technology, ShanghaiTech University, Shanghai 201210, China

[†] These authors contributed equally to this work.

* Correspondence to: Lan Bao, E-mail: baolan@sibcb.ac.cn

Edited by Xuebiao Yao

Microtubules (MTs) are regulated by a number of known posttranslational modifications (PTMs) on α/β -tubulin to fulfill diverse cellular functions. Here, we showed that SUMOylation is a novel PTM on α -tubulin *in vivo* and *in vitro*. The SUMOylation on α -tubulin mainly occurred at Lys 96 (K96), K166, and K304 of soluble α -tubulin and could be removed by small ubiquitin-related modifier (SUMO)-specific peptidase 1. *In vitro* experiments showed that tubulin SUMOylation could reduce interprotofilament interaction, promote MT catastrophe, and impede MT polymerization. In cells, mutation of the SUMOylation sites on α -tubulin reduced catastrophe frequency and increased the proportion of polymerized α -tubulin, while upregulation of SUMOylation with fusion of SUMO1 reduced α -tubulin assembly into MTs. Additionally, overexpression of SUMOylation-deficient α -tubulin attenuated the neurite extension in Neuro-2a cells. Thus, SUMOylation on α -tubulin represents a new player in the regulation of MT properties.

Keywords: α -tubulin, SUMOylation, microtubule dynamics, microtubule assembly

Introduction

Microtubules (MTs) are cytoskeletal filaments that are dynamically assembled from α/β -tubulin heterodimers. α -tubulin and β -tubulin subunits are very similar and highly conserved across all eukaryotic species. MTs play different roles in a variety of biological processes, such as intracellular transport, cell migration (Etienne-Manneville, 2013), chromosome segregation (Wittmann et al., 2001; Glotzer, 2009), and establishment and maintenance of cell polarity (Conde and Caceres, 2009;

Stiess and Bradke, 2011; Rodriguez-Boulan and Macara, 2014). In addition to different tubulin isoforms and various MT-associated proteins, multiple MT functions are achieved through numerous posttranslational modifications (PTMs) on tubulin, including acetylation, dephosphorylation, glutamylation, glycylation, and more recently, polyamination and methylation (Song et al., 2013; Janke, 2014; Park et al., 2016).

SUMOylation is an important PTM involving the covalent conjugation of the small ubiquitin-related modifier (SUMO) to target proteins. This modification, catalyzed through an enzymatic cascade involving E1 (SAE1/2), E2 (Ubc9), and/or E3, regulates the activity or subcellular localization of various proteins and participates in a plethora of cellular processes (Geiss-Friedlander and Melchior, 2007; Henley et al., 2014). Interestingly, in recent studies, a series of cytoskeletal proteins, such as β -actin, keratins, septins, and lamin A, were found to undergo SUMOylation whereby the dynamics of actin

Received November 12, 2020. Revised December 2, 2020. Accepted December 14, 2020.

© The Author(s) (2021). Published by Oxford University Press on behalf of *Journal of Molecular Cell Biology*, CEMCS, CAS.

This is an Open Access article distributed under the terms of the Creative Commons Attribution Non-Commercial License (<http://creativecommons.org/licenses/by-nc/4.0/>), which permits non-commercial re-use, distribution, and reproduction in any medium, provided the original work is properly cited. For commercial re-use, please contact journals.permissions@oup.com

and intermediate filaments were modulated (Zhang and Sarge, 2008; Hofmann et al., 2009; Kaminsky et al., 2009; Snider et al., 2011; Ribet et al., 2017), raising the possibility that SUMOylation might also have a role in regulating additional cytoskeleton components. In line with this, the cytoskeletal protein tubulins have been uncovered as hits in proteomic screening for SUMO substrates in yeast and mammalian cells, and a brief immunoblotting was used to validate the SUMO3 modification on α -tubulin (Panse et al., 2004; Rosas-Acosta et al., 2005). As it is insufficient to confirm the SUMOylation of α -tubulin by a single method (Alonso et al., 2015), and more importantly, little is known about the machinery and function of this novel PTM, further explorations are needed.

Given the emerging roles of SUMOylation in cytoskeleton regulation and the hint from proteomic studies, we further investigated the SUMOylation of α -tubulin and the role of SUMOylation in MT functions. Here, we confirmed that α -tubulin was indeed SUMOylated in cultured cells, with Lys96 (K96), K166, and K304 as major acceptor sites by SUMO1. Importantly, tubulin SUMOylation reduced interprotofilament interaction, promoted MT catastrophe, and impeded MT polymerization *in vitro*. Furthermore, SUMOylation of α -tubulin decreased its incorporation into MTs *in vivo* and was involved in neurite extension in Neuro-2a cells. Collectively, SUMOylation is a novel PTM of α -tubulin that orchestrates MT properties.

Results

α -tubulin is SUMOylated in cells and in vitro

To verify whether α -tubulin was SUMOylated, HEK293 cells were transiently transfected with Flag-SUMO1, Flag-SUMO2, or Flag-SUMO3. Immunoprecipitation (IP) with α -tubulin antibody (α -Tub Ab) clearly showed multiple bands of molecular weight higher than 50 kDa in cells expressing Flag-SUMO1, corresponding to differentially SUMOylated forms of α -tubulin, while only one or two up-shifted weak bands were observed in cells expressing Flag-SUMO2 or Flag-SUMO3 (Figure 1A). Consistently, SUMOylated bands were observed in α -tubulin immunoprecipitates when probed by SUMO1 Ab (Figure 1B). In addition, in HEK293 cells transfected with HA-Ubc9, we found that α -tubulin could be coimmunoprecipitated with Ubc9, the unique E2 enzyme for SUMOylation (Figure 1C), indicating that α -tubulin interacts with the SUMOylation machinery. All above evidence suggested that α -tubulin is a SUMO1-modified substrate in cells. To further validate the SUMOylation of α -tubulin by SUMO1, *in vitro* SUMOylation assay using brain tubulin as substrates was performed. Immunoblotting showed that α -tubulin was SUMOylated in the presence of recombinant SAE1/2, Ubc9, and SUMO1GG (Figure 1D–H), with the ratio of SUMOylated α -tubulin to unSUMOylated being $\sim 7.8\%$ (Figure 1G). Further *in vitro* SUMOylation using MTs and tubulin dimers as substrates showed that α -tubulin in dimers could be more efficiently SUMOylated than that in MTs (Figure 1I), suggesting that α -tubulin SUMOylation is a soluble-tubulin-enriched PTM. We also surveyed the SUMOylation of α -tubulin in several cell lines and mouse tissues, and found that

the level and pattern of α -tubulin SUMOylation varied a lot across cell lines and mouse tissues investigated (Supplementary Figure S1A and B). The α -tubulin SUMOylation in a specific type of cell or tissue may be controlled by the level and activity of all the SUMOylation machinery proteins for α -tubulin, such as E1, E2, E3 (if any), and SUMO-specific peptidase 1 (SEN1), and is compatible with distinct cell property or tissue function. These data indicate that α -tubulin is able to be SUMOylated *in vivo* and *in vitro*.

Because α/β -tubulin constitutively exist as dimers, whether β -tubulin could be SUMOylated was examined. We found that upon SUMO1, SUMO2, or SUMO3 overexpression, β -tubulin was mainly modified by SUMO1 in HEK293 cells (Figure 1J). In addition, β -tubulin could be SUMOylated *in vitro* (Figure 1K). However, SUMOylation of endogenous β -tubulin in cells without SUMO1 overexpression was almost undetectable (Figure 1L). Since the basal level of β -tubulin SUMOylation is low in cells, we mainly focused on the study of α -tubulin SUMOylation.

SUMOylation is mainly enriched in soluble α -tubulin

To determine the localization of SUMOylated α -tubulin, proximity ligation assay (PLA), which enables detection of protein modification *in situ* (Soderberg et al., 2006), was performed using primary antibodies against α -tubulin and SUMO1. Immunostaining showed that PLA signals were located both on MTs and in the cytoplasm, but largely ($\sim 70\%$) distributed in the cytoplasm (Figure 2A and B), suggesting that SUMOylation of α -tubulin may mainly occur on unpolymerized tubulins. To further confirm this phenomenon, soluble and polymerized tubulins were separated in HEK293 cells expressing Flag-SUMO1. Followed SUMOylation detection of these two pools by IP showed that, in line with the PLA results, soluble α -tubulin had a much higher level of SUMOylation than polymerized α -tubulin (Figure 2C and D). The preferential distribution on soluble α -tubulin in cells was consistent with a higher catalytic efficiency of SUMOylation machinery toward soluble tubulins *in vitro* (Figure 1I).

α -tubulin is SUMOylated at K96, K166, and K304 and deSUMOylated by SENP1

To facilitate the following functional studies of α -tubulin SUMOylation, we mapped the SUMO conjugation sites on α -tubulin. Many SUMOylation reactions occur on a consensus motif ψ Kx_nD/E, where ψ represents a large hydrophobic amino acid and x indicates any amino acid (Rodriguez et al., 2001). Because of the highly conserved lysines and similar SUMOylation levels across α -tubulin isoforms (Figure 3A and B), α -tubulin 1A isoform ($\alpha 1A$) was chosen as an example during the site screening. Previous mass spectrometry (MS)-based proteomic screenings predicted that K60, K112, K326, K336, K370, and K401 are potential SUMOylation sites of α -tubulin (Becker et al., 2013; Hendriks et al., 2014; Impens et al., 2014;

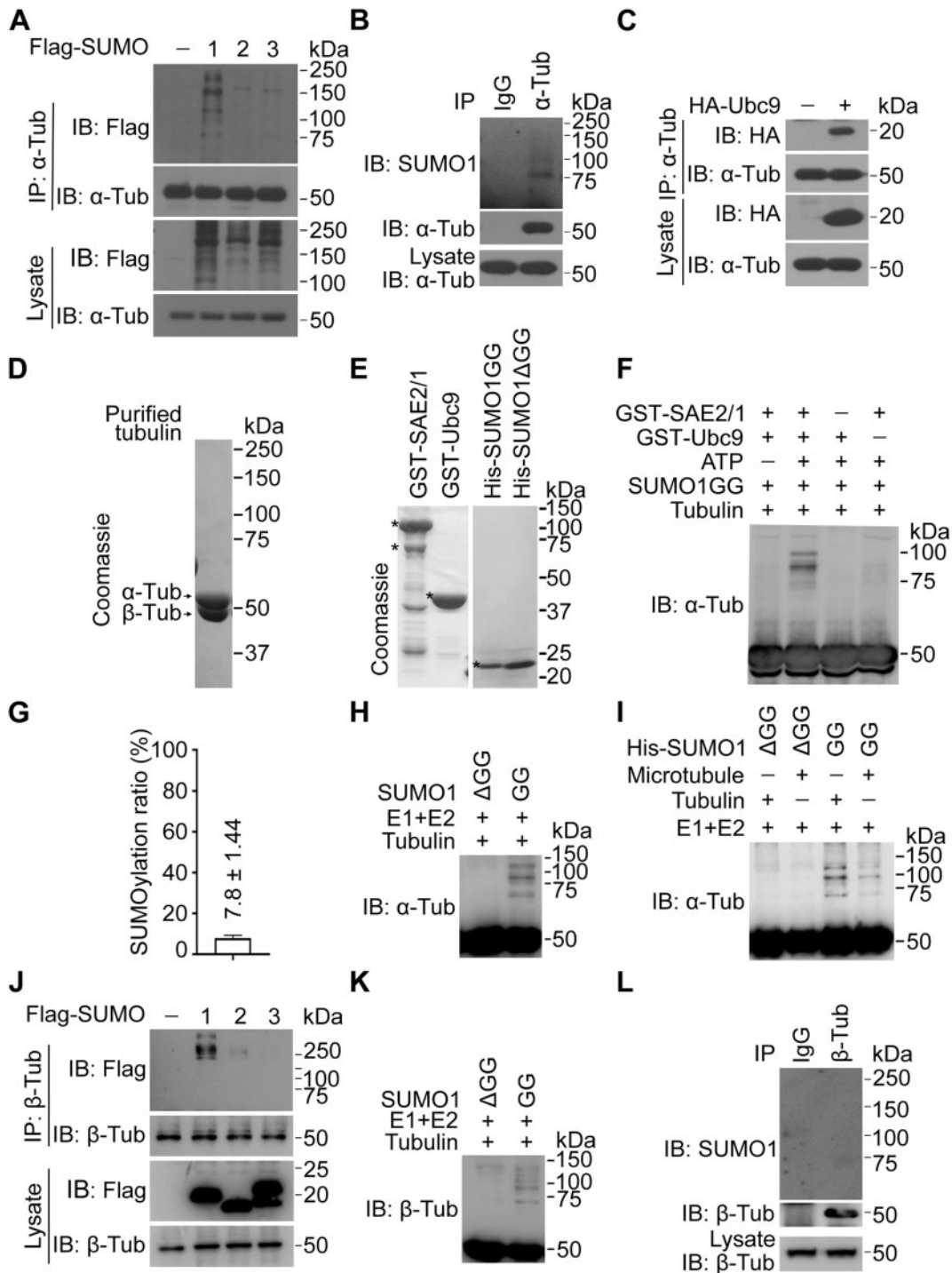


Figure 1 α -tubulin is SUMOylated in cells and *in vitro*. (A) Immunoprecipitates with α -tubulin Ab from HEK293 cells expressing Flag-SUMO1, Flag-SUMO2, or Flag-SUMO3 were subject to immunoblotting (IB) and probed with Flag and α -tubulin (α -Tub) Abs. (B) Endogenous α -tubulin in HEK293 cells was immunoprecipitated and probed with SUMO1 Ab. (C) Immunoprecipitates with α -tubulin Ab from HEK293 cells expressing HA-Ubc9 were probed with HA and α -tubulin Abs. (D) Coomassie blue staining of purified mouse brain tubulin including α -tubulin and β -tubulin, indicated by arrows. (E) Coomassie blue staining of purified GST-SAE2/1, GST-Ubc9, His-SUMO1GG, and His-SUMO1 Δ GG. Asterisk indicates the band of purified protein. (F) *In vitro* SUMOylation assay using purified GST-SAE2/1, GST-Ubc9, His-SUMO1GG, and brain tubulins. (G) Ratio of density of SUMOylated bands to unSUMOylated bands. (H) Purified tubulin was *in vitro* SUMOylated and probed with α -tubulin Ab. (I) *In vitro* SUMOylation assay using soluble tubulins and MTs. (J) Immunoprecipitates with β -tubulin Ab from HEK293 cells expressing Flag-SUMO1, Flag-SUMO2, or Flag-SUMO3 were probed with Flag and β -tubulin Abs. (K) Purified tubulin was *in vitro* SUMOylated and probed with β -tubulin Ab. (L) Endogenous β -tubulin in HEK293 cells was immunoprecipitated and probed with SUMO1 Ab. The experiments were repeated three times.

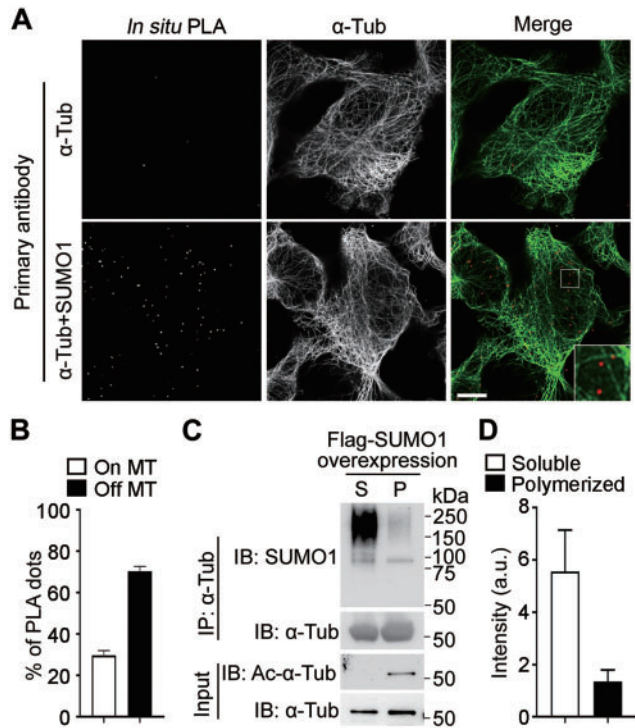


Figure 2 SUMOylation is mainly enriched in soluble α -tubulin. (A) PLA with α -tubulin and SUMO1 Abs was performed in HEK293 cells. Confocal images of PLA signals and tubulin labelled after PLA are shown. The enlarged image of the boxed area is shown at the lower right. Scale bar, 10 μ m. (B) PLA dots on and off MTs were quantified. $n = 11$ cells. (C) Soluble and polymerized tubulins were separated in SUMO1-overexpressing HEK293 cells and subject to IP using α -tubulin Ab. Immunoprecipitates were detected by SUMO1 Ab. The experiments were repeated three times. (D) Quantification of the SUMOylation in soluble or polymerized tubulins. Data are mean \pm SEM from three independent experiments.

Lumpkin et al., 2017). However, neither mutating these lysines to arginines individually nor jointly (MS-6KR) could significantly reduce α -tubulin SUMOylation (Figure 3C). Therefore, we next turned to bioinformatic tools. Bioinformatic analysis by several softwares, including GPS-SUMO 1.0, SUMOsp 2.0, JASSA, and SUMOgo (Ren et al., 2009; Zhao et al., 2014; Beauclair et al., 2015; Chang et al., 2018), predicted that K96, K166, and K304 of α -tubulin were putative sites for SUMO conjugation (Figure 3D). IP showed that single mutation of each lysine into arginine (K96R, K166R, K304R) or double mutation (K96,166R; K96,304R; K166,304R) had little influence on the level of α -tubulin SUMOylation in HEK293 cells expressing HA-SUMO1. However, simultaneously mutating K96, K166, and K304 into arginine (K96,166,304R; 3KR) nearly completely abolished α 1A SUMOylation (Figure 3E). Thus, K96, K166, and K304 are major sites of α -tubulin SUMOylation.

In the structure of α/β -tubulin dimer, K96, K166, and K304 were scattered on α -tubulin (Figure 3F). Notably, K96 located close to

H2-S3 loop and K304 located close to the M-loop (S7-H9 loop) (Figure 3G), both of which are key components involved in lateral contacts between protofilaments (Zhang et al., 2015), raising the possibility that once incorporated into MTs, SUMOylated α -tubulin may impair the interprotofilament interaction.

Since previous study reported that SUMO1 could be multimerized via its K7, K16, and K17 and conjugated to substrates *in vitro* (Pedrioli et al., 2006), we tested whether α -tubulin conjugates contained SUMO1 multimer. IP showed that mutating above lysine into arginine on SUMO1 did not change the pattern of α -tubulin SUMOylation (Figure 3H), implying lack of K7, K16, and K17-mediated SUMO1 multimer. These α -tubulin conjugates, present in both cell lines and mouse tissues, suggest that α -tubulin has a complex pattern of SUMOylation *in vivo*.

SUMOylation is a dynamic PTM that can be reversed by SUMO proteases *in vivo* (Henley et al., 2014). Co-IP showed that SENP1 interacted with α -tubulin and overexpressing SENP1 dramatically reduced the SUMOylation level of α -tubulin in HEK293 cells (Figure 3I and J). Furthermore, deletion of SENP1 in mouse brain at E13.5 significantly upregulated α -tubulin SUMOylation (Figure 3K). This result reveals an important role of SENP1 in balancing the SUMOylation level *in vivo*.

α -tubulin SUMOylation promotes MT catastrophe

Since SUMOylation of α -tubulin was validated, the role of this modification in regulating MT properties was examined using a series of *in vitro* methods. Because the steady-state level of SUMOylation for most proteins was very low (Geiss-Friedlander and Melchior, 2007), highly purified tubulins (Figure 1D), obtained by two cycles of assembly–disassembly under harsh conditions to minimize binding proteins and related interference (Castoldi and Popov, 2003), were *in vitro* SUMOylated as above mentioned (Figure 1F) and used in different analysis. In turbidity assay, compared to control tubulins prepared by *in vitro* reaction without E2 (–E2), SUMOylated tubulins reached a relatively lower polymerization level (Figure 4A). Thus, tubulin SUMOylation reduces MT assembly.

To dissect the influence of SUMOylation on MT dynamics in detail, MT reconstitution assay was performed using *in vitro* SUMOylated tubulins (Figure 4B). The dynamics of MT plus ends, including MT growth and catastrophe (transition from growth to rapid shrinkage), were recorded by total internal reflection fluorescence (TIRF) microscopy. Tubulins prepared by reactions without E2 (–E2) were used as a control in this assay. As demonstrated by the representative kymographs, typical MT growth and catastrophe events could be observed in both groups (Figure 4C and D). Quantification of MT dynamics showed that after tubulin SUMOylation, catastrophe frequency of MTs was significantly increased, growth rate was unchanged, and thus the maximum length of MTs was significantly reduced (Figure 4E). Moreover, tubulins prepared by reaction with conjugation-defective SUMO1 Δ GG were used as another control (SUMO1 Δ GG). Quantitative data pointed to the similar conclusion that tubulin SUMOylation enhances MT catastrophe but does not affect growth

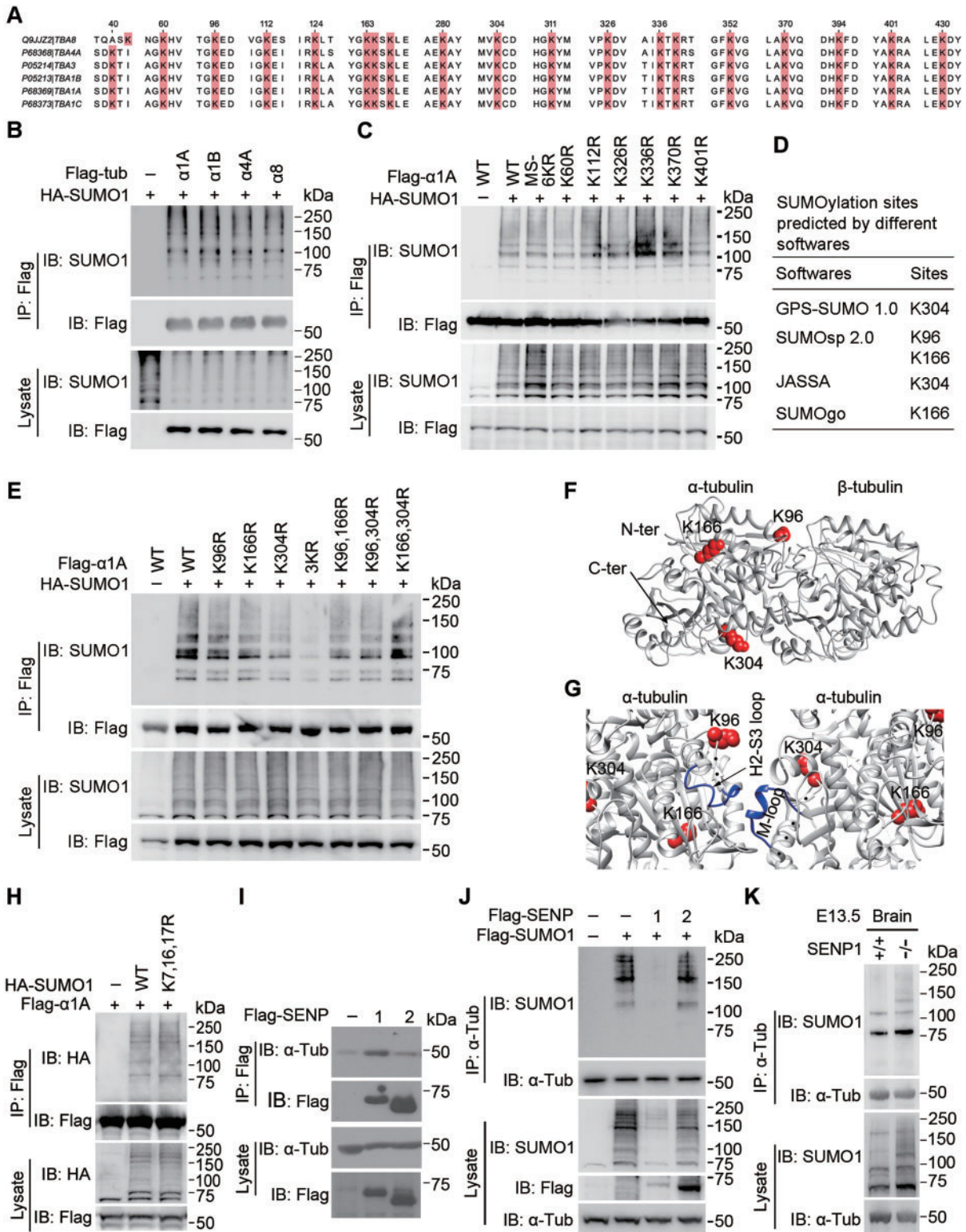


Figure 3 α-tubulin is SUMOylated at K96, K166, and K304 and deSUMOylated by SENP1. (A) Alignment of lysines (in red color) and surrounding sequences of α-tubulin isoforms in the mouse. (B) Immunoprecipitates with Flag M2 beads from HEK293T cells expressing HA-SUMO1 with Flag-tagged isoforms of α-tubulin as indicated were probed with SUMO1 and Flag Abs. (C) Flag-tagged wild-type (WT) and various α1A mutant at MS-predicted SUMOylation sites were expressed with HA-SUMO1 in CHO-K1 cells and then immunoprecipitated. Immunoprecipitates were detected by SUMO1 and Flag Abs. (D) List of putative SUMOylation sites on α1A isoform predicted by different softwares. (E) Flag-tagged WT and combined mutant α1A at bioinformatics-predicted SUMOylation sites were expressed with HA-SUMO1 in

rate (Figure 4F). Collectively, these data suggest that tubulin SUMOylation elevates the dynamic instability.

The assembly of MTs as a multistep process mainly includes the formation of short protofilaments from α/β -tubulin dimers through longitudinal interactions and the association of small sheets through parallel interprotofilament interactions into hollow tubules. Hence, MT dynamics is governed by longitudinal and lateral tubulin interactions. Based on the structure of MTs (Vemu et al., 2016), the SUMO-acceptor sites (K96 and K166) are proximal to the lateral interface between protofilaments (Figure 3G). Therefore, protofilament formation and association assays (Portran et al., 2017) were performed to detect the longitudinal and lateral interactions between α/β -tubulin dimers after *in vitro* SUMOylation, respectively. The protofilament formation assay did not show a difference in the curvature and length of protofilaments between SUMOylated and control tubulins (Figure 4G). However, the protofilament association assay revealed that SUMOylated tubulin sheets contained less protofilaments than control tubulin sheets (Figure 4H), indicating that tubulin SUMOylation weakens the lateral interactions between protofilaments.

Our *in vitro* assays showed that tubulin SUMOylation could promote catastrophe frequency. However, the effect may result from SUMOylation of both α -tubulin and β -tubulin. Since the basal SUMOylation of β -tubulin is almost undetectable and only α -tubulin is SUMOylated, we wonder whether α -tubulin SUMOylation alone could promote catastrophe in cells. To address this question, we studied the effect of α 1A(3KR) on MT dynamics using time-lapse imaging in cells expressing EB3-tdTomato. Results showed that overexpressing α 1A(3KR) reduced MT catastrophe frequency (0.32 ± 0.01 to $0.28 \pm 0.01 \text{ sec}^{-1}$) but had no influence on growth rate (Figure 4I), suggesting that α -tubulin SUMOylation could promote MT catastrophe.

α -tubulin SUMOylation impedes its assembly into MTs in cells

Since α -tubulin SUMOylation regulates MT dynamics, we next determined whether α -tubulin SUMOylation could affect overall MT assembly in cells. To directly address the question, we constructed a fusion protein consisting of SUMO1 attached to the N-terminal of α -tubulin (Flag-S1- α 1A), a widely used strategy in the functional study of SUMOylation (Ribet et al., 2017; Lee et al., 2018; Zhou et al., 2018), to partially mimic the SUMOylated form of α -tubulin. Immunostaining showed that Flag-S1- α 1A largely existed in a diffused pattern in the

cytoplasm and formed a less prominent MT network than Flag- α 1A did (Figure 5A). In parallel, biochemical fractionation of soluble and polymerized tubulins revealed that a smaller ratio of Flag-S1- α 1A was distributed in the polymerized fraction (Figure 5B). Since Flag- α 1A was well incorporated into MTs and expression levels of Flag- α 1A and Flag-S1- α 1A were very similar (Supplementary Figure S2A), the reduced incorporation of Flag-S1- α 1A most probably resulted from its conjugation with SUMO1. In summary, these results imply that SUMOylated α -tubulin is less incorporated into MTs in cells.

Since SUMO1-fusion protein lacks dynamicity and site specificity, the effect of SUMOylation on MT dynamics was also studied using SUMOylation-defective mutant α 1A(3KR). Co-IP revealed that the association of Flag- α 1A(3KR) with β -tubulin was similar to that of Flag- α 1A and Flag-S1- α 1A (Figure 5C), suggesting that 3KR mutation and SUMO1 fusion do not affect tubulin dimerization. Immunostaining showed that the SUMOylation-defective mutant α 1A(3KR) was able to incorporate into MTs in HEK293 cells (Figure 5D). Further biochemical fractionation showed that the ratio of polymerized tubulin to soluble tubulin (P/S) was larger in α 1A(3KR) mutant than in wild-type α 1A (Figure 5E). Meanwhile, the pelleted α 1A(3KR) was sensitive to nocodazole, indicating that it was a polymerized MT but not protein aggregate (Figure 5F). Therefore, mutating α -tubulin SUMOylation sites increased MT assembly. Given that K96, K166, and K304 were also putative sites for acetylation or ubiquitination (<https://www.phosphosite.org>), we compared these PTMs on α 1A and α 1A(3KR), and no difference was observed in acetylation or ubiquitination between them (Figure 5G and H). Moreover, both α 1A and α 1A(3KR) could bind to SUMO1 molecules similarly (Supplementary Figure S2B), implying that the influence of 3KR on MT polymerization was not due to abnormal noncovalent interaction with SUMO1. Altogether, these data suggest that SUMOylation of α -tubulin could decrease its incorporation into MTs in cells. This is also evidenced by the fact that SUMO1 fusion to the N-terminal of α 1A(3KR) eliminated its distribution preference in the polymerized fraction (Figure 5I), suggesting that the SUMO conjugation was sufficient to reduce α -tubulin incorporation into MTs.

α -tubulin SUMOylation facilitates neurite extension in Neuro-2a cells

Coordinated MT dynamics is essential for the neurite outgrowth, extension, and branching in developing neurons (Sakakibara

CHO-K1 cells and then immunoprecipitated. Immunoprecipitates were detected by SUMO1 and Flag Abs. (F) Schematic representation of SUMOylation sites on the structure of α -tubulin. K96, K166, and K304 are shown as red spheres. (G) Location of SUMOylation sites and the interface for lateral contact between two α -tubulins in one MT. K96, K166, and K304 are shown as red spheres, and H2-S3 loop and M-loop are in blue. (H) Flag- α 1A was overexpressed with HA-SUMO1 or HA-SUMO1-K7,16,17R mutant in HEK293 cells. Immunoprecipitates using Flag M2 beads were probed with HA and Flag Abs. (I) Immunoprecipitates with Flag M2 beads from HEK293 cells expressing Flag-SENP1 or Flag-SENP2 were probed with Flag and α -tubulin Abs. (J) Immunoprecipitates with α -tubulin from HEK293 cells expressing Flag-SENP1 or Flag-SENP2 with Flag-SUMO1 were probed with SUMO1 and α -tubulin Abs. (K) Immunoprecipitates from E13.5 brain of *SENP1*^{+/+} and *SENP1*^{-/-} mice were probed with SUMO1 and α -tubulin Abs. The experiments were repeated three times.

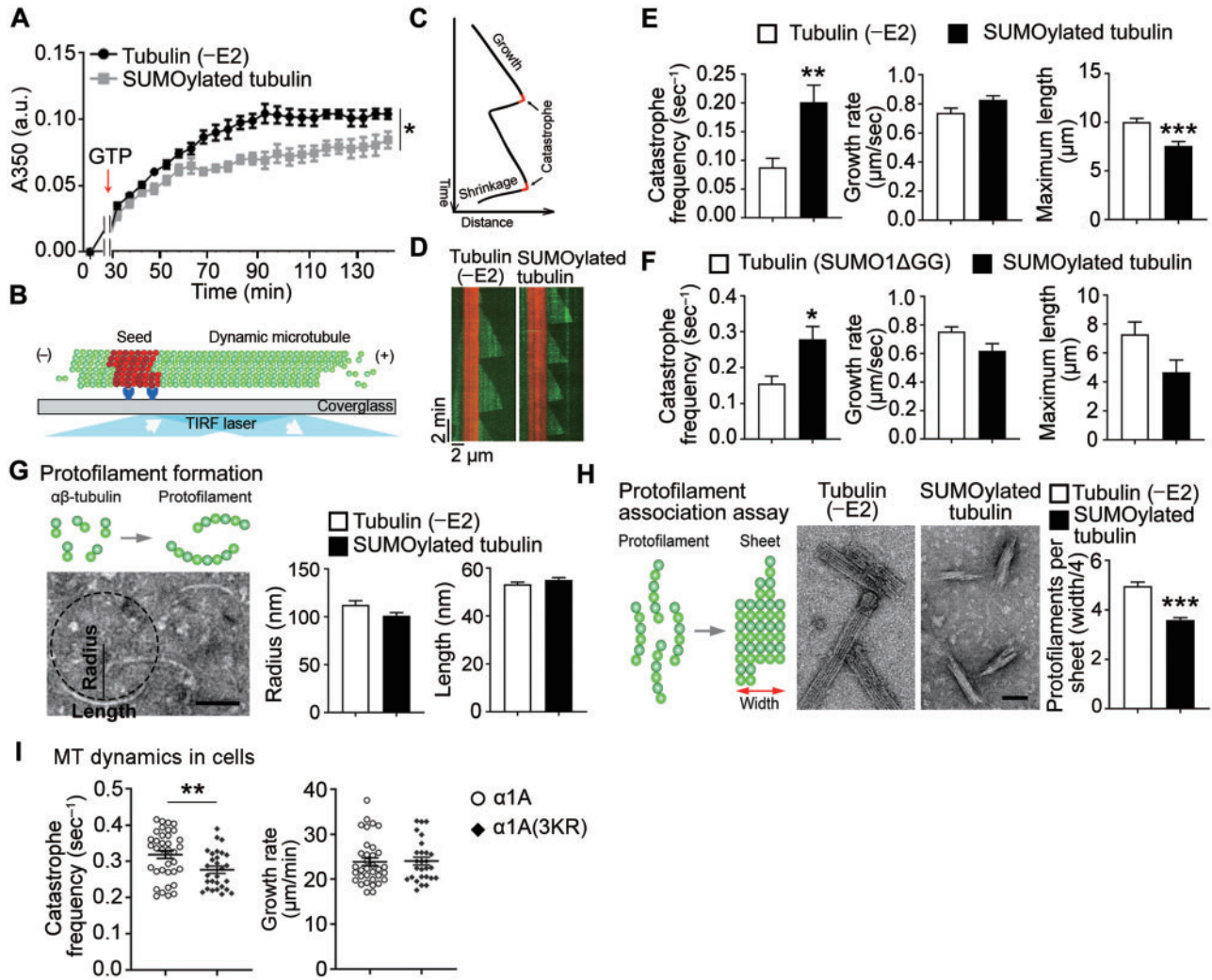


Figure 4 α -tubulin SUMOylation attenuates MT polymerization *in vitro* and in cells. **(A)** MT polymerization with control (-E2) and SUMOylated tubulins was monitored with absorbance at 350 nm (A350). a.u., arbitrary unit. $n = 3$. $*P < 0.05$ vs. control (-E2) tubulin, by Student's *t*-test. **(B)** Schematic illustration of the *in vitro* reconstitution of dynamic MTs. Dynamic MT (in green) grown from the plus end of immobilized seeds (in red) was imaged by TIRF microscopy. **(C)** Illustration of different events of MT dynamics. Dynamic MTs undergo cycles of growth (MT extension) and shrinkage (MT shortening). The transition from growth to shrinkage was catastrophe (red turn). **(D)** Representative kymographs of MT dynamics reconstituted with control (-E2) and SUMOylated tubulins. MT seeds are in red and the dynamic MTs are in green. Scale bar, 2 μ m (horizontal) and 2 min (vertical). **(E)** Catastrophe frequency, growth rate, and maximum length of MT dynamics reconstituted with control (-E2) and SUMOylated tubulins were quantified. For control (-E2) and SUMOylated tubulins, $n = 9$ independent experiments including 80–160 MTs. $**P < 0.01$ and $***P < 0.001$ vs. control (-E2) tubulin, by Student's *t*-test. **(F)** Catastrophe frequency, growth rate, and maximum length of MT dynamics reconstituted with control (SUMO1 Δ GG) and SUMOylated tubulins were quantified. For control (SUMO1 Δ GG) and SUMOylated tubulins, $n = 3$ independent experiments including 150–180 MTs. $*P < 0.05$ vs. control (SUMO1 Δ GG) tubulin, by Student's *t*-test. **(G)** Protofilament formation assay followed by detection with negative-stain electron microscopy was performed, and the length and radius of each protofilament were measured. A circle was fitted to a protofilament for radius measurement. Scale bar, 50 nm. For control (-E2) and SUMOylated tubulins, $n = 491$ and 487 protofilaments from three independent experiments, respectively. Mann-Whitney test was used. **(H)** Protofilament association assay followed by detection of negative-stain electron microscopy was performed. Representative pictures are shown. Scale bar, 50 nm. The protofilament number per sheet was obtained by dividing the width of tubulin sheet with the mean width (4 nm) of a protofilament. For control (-E2) and SUMOylated tubulins, $n = 319$ and 289 sheets from three independent experiments, respectively. $***P < 0.001$ vs. control (-E2) tubulin, by Mann-Whitney test. Data are represented as mean \pm SEM. **(I)** HEK293 cells expressing pCAG- α 1A-IRES-GFP or pCAG- α 1A(3KR)-IRES-GFP with EB3-tdTomato were imaged. Growth rate and catastrophe frequency were quantified. $n = 37$ cells for pCAG- α 1A-IRES-GFP and $n = 28$ cells for pCAG- α 1A(3KR)-IRES-GFP. $**P < 0.01$ vs. pCAG- α 1A-IRES-GFP, by Student's *t*-test.

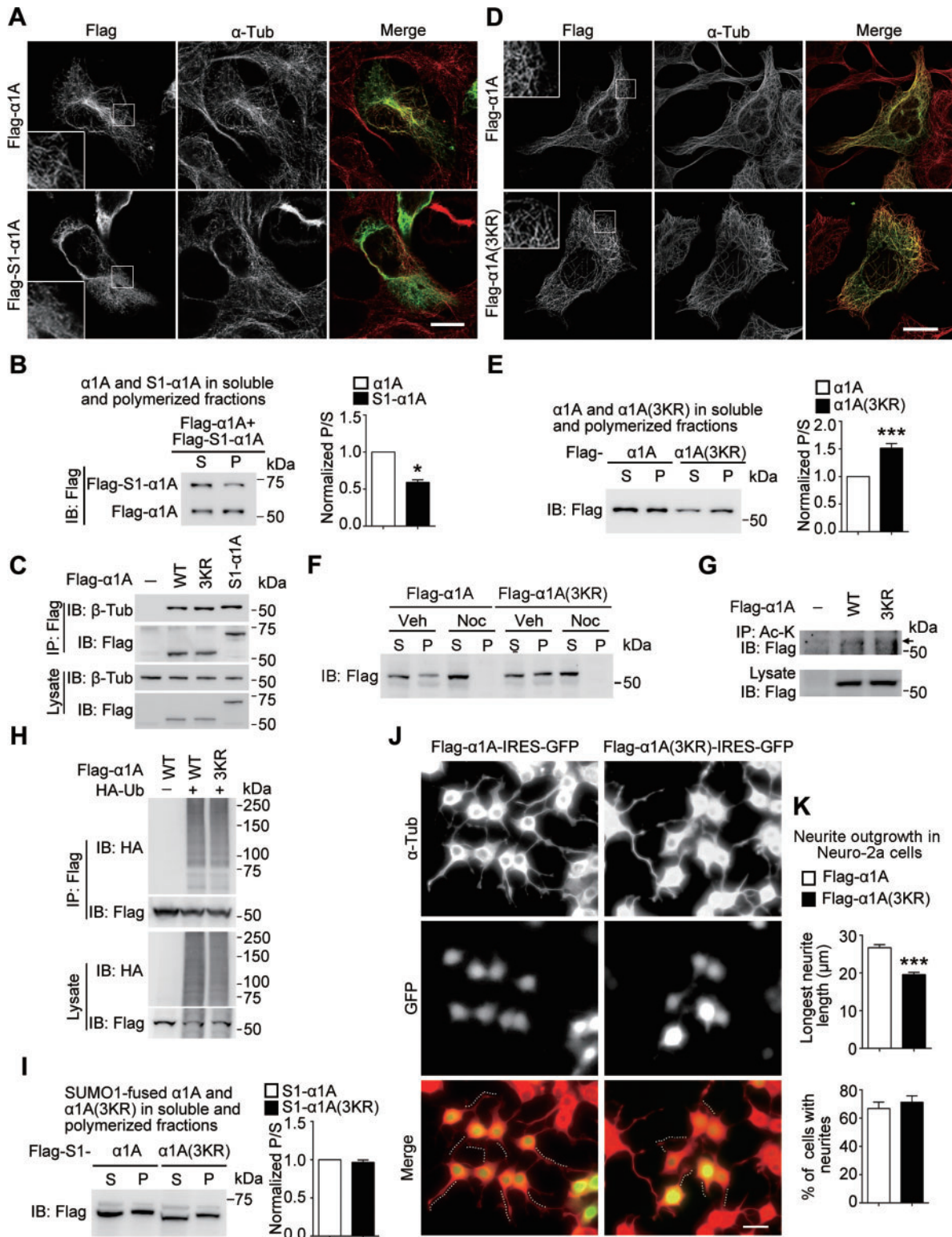


Figure 5 α -tubulin SUMOylation reduces its assembly into MTs in cells and facilitates neurite extension in Neuro-2a cells. **(A)** Flag- α 1A or Flag-S1- α 1A was expressed in HEK293 cells and stained with Flag and α -tubulin Abs. Representative images are shown. The enlarged image of the boxed area is shown at the lower left. Scale bar, 10 μ m. **(B)** Flag- α 1A and Flag-S1- α 1A were coexpressed in HEK293 cells. Soluble (S) and polymerized (P) tubulins were separated and probed with Flag Ab. The ratio of polymerized tubulin to soluble tubulin (P/S) was calculated. $*P < 0.05$ vs. Flag- α 1A, by Student's *t*-test. **(C)** Flag- α 1A, Flag- α 1A(3KR), and Flag-S1- α 1A were overexpressed in HEK293 cells, immunoprecipitated with Flag beads, and immunoblotted with β -tubulin Ab. **(D)** Flag- α 1A or Flag- α 1A(3KR) was expressed in HEK293 cells and stained

et al., 2013). To test whether α -tubulin SUMOylation was involved in this process, we examined the effect of SUMOylation-deficient α 1A(3KR) on the neurite growth in Neuro-2a cells, a widely used cell line capable of developing neurites upon serum deprivation (Shea et al., 1985). Immunostaining and quantitative data showed that, compared to Neuro-2a cells expressing wild-type α 1A, the neurite extension was significantly reduced by \sim 25% in cells expressing α 1A(3KR), while the ratio of neurite-bearing cells was similar (Figure 5J and K). Therefore, α -tubulin SUMOylation is involved in the process of neurite extension.

Discussion

SUMOylation has recently emerged as an important PTM involved in diverse cellular processes. In this study, we identified SUMOylation as a *bona fide* PTM of α -tubulin. In the presence of moderate α -tubulin SUMOylation, a proper level of tubulin polymerization is maintained. However, when α -tubulin SUMOylation is abrogated, more tubulins partition into MTs, indicating an increased formation of MTs and impaired MT dynamics. Our study, together with other reports of the SUMO-regulated cytoskeletal components (Hofmann et al., 2009; Kaminsky et al., 2009; Alonso et al., 2015; Ribet et al., 2017), adds new knowledge to understanding the roles of SUMOylation in orchestrating cytoskeletal dynamics.

It is believed that SUMO1 is conjugated as a monomer due to its lack of the consensus motif (ψ KxD/E) required for next SUMO1 conjugation (Tatham et al., 2001). In our experiments, the bands of higher molecular weight probably represent mono-SUMOylated α -tubulin at multiple lysine residues, which is in accordance with the findings that K96, K166, and K304 are together to serve as major SUMOylation sites and SUMO1-K7,16,17R mutant does not affect SUMOylation pattern. However, possibility still exists that SUMO1 is conjugated to other nonconsensus lysines on SUMO1 to form chains (Ulrich, 2008). Therefore, the content of high molecular weight conjugates of α -tubulin SUMOylation is still an open question.

Using PLA assay and biochemical separation, we found that the majority of SUMOylated α -tubulin predominantly exists in the soluble form, and only a small amount locates on MTs. The distribution pattern of SUMOylated α -tubulin is compatible to

its anti-polymerization role. To be specific in cells, SUMOylated α -tubulins display a very low capacity to incorporate into MTs; once SUMOylated α -tubulins are incorporated into MTs, they promote MT catastrophe and cause MT disassembly.

Mapping of the three SUMOylation sites on the crystal structure of α/β -tubulin dimers showed that K96 and K304 located close to the key components involved in the lateral contacts (Nogales et al., 1998; Zhang et al., 2015), pointing to a potential role of SUMOylation in inhibiting tubulin assembly into MTs by weakening lateral interaction. This postulation matches the *in vitro* results that α -tubulin SUMOylation led to a reduction in the lateral interaction between protofilaments. Given the previous view that MT catastrophe is triggered when the lateral contact fails to counteract longitudinal strain (Manka and Moores, 2018), α -tubulin SUMOylation decreases the interprotofilament interaction, and thus leads to MT catastrophe.

Generally, various known PTMs of tubulins control MT dynamics within cells in two ways: altering tubulin properties or changing the interaction with MT-associated proteins or motor proteins (Janke and Bulinski, 2011; Magiera et al., 2018). The reduced interprotofilament interaction and the increased catastrophe frequency of MTs observed in *in vitro* experiments after tubulin SUMOylation most probably resulted from alterations in tubulin itself. These *in vitro* effects could provide one of the possible explanations for the cellular phenotypes of α -tubulin SUMOylation. Meanwhile, α -tubulin SUMOylation may also modulate MT dynamics indirectly via MT-associated proteins or motor proteins in cells. For example, ubiquitinated α -tubulin was found to interact with intraflagellar transport protein for retrograde transport during ciliary disassembly in *Chlamydomonas* (Wang et al., 2019). Considering the similarity between ubiquitination and SUMOylation, it will be very interesting to determine whether SUMOylation changes the interaction partners of tubulin, which may provide further insights into the regulation of MT functions by α -tubulin SUMOylation.

In the present study, SUMOylation-deficient α -tubulin, which displayed abnormal MT dynamics, i.e. decreased MT catastrophe, resulted in reduced neurite extension in Neuro-2a cells. These phenomena quite resemble the previous finding that pharmacological manipulation with high doses of taxol is sufficient to block MT dynamics and neurite extension in cultured neurons (Letourneau and Ressler, 1984; Dehmelt et al., 2003;

with Flag and α -tubulin Abs. Representative images are shown. The enlarged image of the boxed area is shown at the upper left. Scale bar, 10 μ m. (E) Flag- α 1A or Flag- α 1A(3KR) was expressed in HEK293 cells. Soluble and polymerized tubulins were separated and probed with Flag Ab. The P/S ratio was calculated. $***P < 0.001$ vs. Flag- α 1A, by Student's *t*-test. (F) Flag- α 1A or Flag-S1- α 1A(3KR) was expressed in HEK293 cells and treated with 5 μ M nocodazole for 30 min. Soluble and polymerized tubulins were separated and probed with Flag Ab. (G) Flag- α 1A or Flag- α 1A(3KR) was overexpressed in HEK293 cells. Lysates were immunoprecipitated with pan-Ac-K Ab and immunoblotted with Flag Ab. (H) Flag- α 1A, Flag- α 1A(3KR), and HA-Ub were overexpressed in HEK293 cells. Lysates were immunoprecipitated with Flag beads and immunoblotted with HA Ab. (I) Flag-S1- α 1A or Flag-S1- α 1A(3KR) was expressed in HEK293 cells. Soluble and polymerized tubulins were separated and probed with Flag Ab. The P/S ratio was calculated. Student's *t*-test was used. (J) Neuro-2a cells expressing Flag- α 1A-IRES-GFP or Flag- α 1A(3KR)-IRES-GFP were induced for differentiation by serum deprivation for 3 h and stained with α -tubulin Ab. Representative images are shown. Dashed lines indicate the longest neurite of each cell. Scale bar, 20 μ m. (K) Quantification of the longest neurite length for each cell and the percentage of cells with neurites. $n = 410$ cells for Flag- α 1A-IRES-GFP and $n = 438$ cells for Flag- α 1A(3KR)-IRES-GFP. $***P < 0.001$ vs. Flag- α 1A-IRES-GFP, by Mann-Whitney test. Data from three independent experiments are represented as mean \pm SEM.

Witte et al., 2008), further supporting the importance of coordinated MT dynamics in neurite growth. Considering the high level of α -tubulin SUMOylation in E13.5 mouse brain and its effect in regulating neurite extension in Neuro-2a cells, the role of α -tubulin SUMOylation in brain development will be an interesting topic for further study.

Materials and methods

Mouse

All studies were approved by the Committee of Use of Laboratory Animals and Common Facility, Shanghai Institute of Biochemistry and Cell Biology, Chinese Academy of Sciences. *SENP1*^{-/-} mice were used in our previous study (Cheng et al., 2007). Mice were housed under standard condition in the Animal Core Facility, Shanghai Institute of Biochemistry and Cell Biology, Chinese Academy of Sciences.

Plasmid construction

All primers used for the construction of plasmids expressing tubulin α 1A, α 1B, α 4A, α 8, and α 1A mutations, SUMO1, SUMO1GG, SUMO1 Δ GG (C-terminal di-GG motif deleted to prevent conjugation), SUMO1-K7,16,17R, SUMO2, and SUMO3 are listed in [Supplementary Table S1](#).

The cDNA of rat tubulin α 1A was cloned into pFlag-C2 (pEGFP-C2 backbone with EGFP replaced by Flag) and pCAG-IRES-GFP vectors for the expression of Flag- α 1A and α 1A (with a separately expressed EGFP), respectively. Flag- α 1A mutations were introduced using KOD-plus Mutagenesis Kit (Toyobo). The cDNAs of mouse tubulin α 1A, α 1B, α 4A, α 8, and human SUMO1 were cloned into pCMV-Flag or pCMV-HA vector to express Flag- α 1A, Flag- α 1B, Flag- α 4A, Flag- α 8, Flag-SUMO1 or HA-SUMO1. The cDNAs of human Ubc9 were cloned into pCMV-HA vector for the expression of HA-Ubc9. HA-SUMO1 was obtained by mutating Flag into HA. The cDNAs of SAE2/1 and Ubc9 were cloned into pGEX-4T vector for the expression of GST-SAE2/1 and GST-Ubc9. cDNA of SUMO1GG or SUMO1 Δ GG was cloned into pET-30A vector for the expression of His-SUMO1GG or His-SUMO1 Δ GG. The cDNA encoding SUMO1 Δ GG was inserted to Flag- α 1A or Flag- α 1A(3KR) to produce Flag-SUMO1 Δ GG- α 1A (Flag-S1- α 1A) or Flag-SUMO1 Δ GG- α 1A(3KR) (Flag-S1- α 1A(3KR)). SENP1 and SENP2 were cloned into pFlag-CMV vector.

Cell culture and transfection

Mycoplasma-free HEK293, HEK293T, and Neuro-2a cells (American Type Culture Collection) were cultured in DMEM (GIBCO) supplemented with 10% fetal bovine serum (Biocrom), 1% Penicillin–Streptomycin (GIBCO), and mycoplasma prevention reagent (Yeasten). CHO-K1 cells were cultured in Ham's F-12 medium (GIBCO) supplemented with 10% fetal bovine serum, 1% Penicillin–Streptomycin, and mycoplasma prevention reagent. HEK293, HEK293T, Neuro-2a, and

CHO-K1 cells were transiently transfected using Lipofectamine 2000 (Invitrogen) and harvested for different assays after 24 h.

Co-IP and immunoblotting

Cells or tissues were washed, lysed in lysis buffer (50 mM Tris–HCl, pH 7.5, 150 mM NaCl, 1% Triton X-100, 1 mM EDTA, and 10% glycerol) supplemented with protease inhibitors (1 mM PMSF, 1 μ g/ml pepstatin A, 1 μ g/ml aprotinin, and 1 μ g/ml leupeptin) at 4°C for 30 min, and centrifuged at 16000 *g* at 4°C for 15 min. Supernatants were collected and subject to IP with Flag M2 beads (Sigma-Aldrich) or α -tubulin Ab (Sigma-Aldrich, T9026) at 4°C for 5 h or overnight. The immunoprecipitates and 5%–10% total lysates were processed for immunoblotting.

For the detection of α -tubulin SUMOylation *in vivo*, cells in a 6-cm dish were lysed with 100 μ l denaturing buffer (50 mM Tris–HCl, 1% sodium dodecyl sulphate (SDS)) supplemented with 10 mM NEM (Sigma-Aldrich), heated at 95°C for 10 min, and diluted with lysis buffer to 1 ml. After centrifugation, supernatants were collected and immunoprecipitated with Flag M2 beads or indicated antibodies.

The samples were separated by SDS–polyacrylamide gel electrophoresis, transferred, probed with specific antibodies, and visualized with enhanced chemiluminescence (Tanon). The primary antibodies included mouse antibodies against SUMO1 (1:1000; CST, 4940S), SUMO2/3 (1:1000; CST, 4971S), α -tubulin (1:10000; Sigma, T9026), α -tubulin (1:10000; Abcam, ab18251), Flag (1:10000; Sigma, F7425), β -actin (1:50000; Chemicon, MAB1501), and GAPDH (1:10000; Abcam, ab8245). The immunoreactive bands were quantified using ImageJ (National Institutes of Health).

Separation of soluble and polymerized tubulins

Soluble tubulin and insoluble MTs were separated as described previously with minor modifications (Tanaka et al., 2012). Briefly, cells were lysed in MT stabilization buffer (85 mM PIPES, pH 6.9, 1 mM EGTA, 1 mM MgCl₂, 10% glycerol, 1 μ M Taxol, 0.5% (v/v) Triton X-100, protease inhibitor mixture) at 37°C for 5 min in the dark, and then centrifuged at 17400 *g* for 10 min at room temperature. After the supernatant was transferred to new tubes, the pellets were washed with the MT stabilization buffer without detergents or inhibitors, and then resuspended with BRB80 buffer (80 mM PIPES, pH 6.8, 1 mM MgCl₂, and 1 mM EGTA) for further IP or denatured with SDS sample buffer. Different fractions were then subject to immunoblotting.

Protein purification and *in vitro* SUMOylation assay

Protein purification for human GST-SAE2/1, GST-Ubc9, and His-SUMO1 and *in vitro* SUMOylation assay have been described previously (Vethantham and Manley, 2009). *Escherichia coli* BL21 was transformed with GST-SAE2/1, GST-Ubc9, and His-SUMO1, and protein expression was induced by 1 mM

isopropyl- β -D-thiogalactoside (Amersco) at 30°C for 8 h. The expressed protein was purified using a column packed with bed resin of glutathione-Sepharose beads (Amersham Biosciences) and concentrated using Amicon Ultra4 (5000 molecular weight cutoff concentrators; Millipore). Concentrations of purified proteins were determined by Bradford assay.

Unless otherwise specified, *in vitro* tubulin SUMOylation assay was performed in a 20- μ l volume containing 1 μ g GST-SAE1/SAE2, 1 μ g GST-Ubc9, 1 μ g His-SUMO1, 2 mM 10 \times ATP, and 5–20 μ g tubulins in BRB80 buffer at 37°C for 0.5–1 h. Then, the reaction mixture was denatured to stop reactions by adding SDS sample buffer or used in different assays. Control tubulins were obtained from *in vitro* reactions without E2 or addition of SUMO1 Δ GG.

Immunocytochemistry and in situ PLA

HEK293 or Neuro-2a cells were fixed with methanol at –20°C for 10 min and stained overnight at 4°C with antibodies against Flag (1:500, Origene) and α -tubulin (1:1000; Abcam), followed by donkey anti-mouse IgG (H+L), Alexa Fluor 488 (1:500; Thermo Fisher Scientific) and donkey anti-rabbit IgG (H+L), Alexa Fluor 555 (1:500; Thermo Fisher Scientific) at room temperature for 1–2 h. Next, cells were mounted and imaged with Leica TCS SP8 confocal microscopy with a 60 \times objective lens. The longest neurites of Neuro-2a cells were traced and measured using the NeuronJ plugin in FIJI, a distribution of ImageJ.

In situ PLA was performed according to the manufacturer's instructions (Sigma-Aldrich). Briefly, HEK293 cells were fixed with methanol at –20°C for 5 min. Fixed cells were incubated with primary antibodies against α -tubulin (1:1000, Sigma-Aldrich) with or without SUMO1 (1:500, Cell Signaling Technology) overnight at 4°C, followed with secondary antibodies conjugated with oligonucleotides at 37°C for 1 h and incubated with the ligase in the ligation solution at 37°C for 30 min. After washes, rolling-circle amplification was performed using the polymerase at 37°C for 100 min in the dark. After above reaction, cells were further incubated with primary antibodies against tubulin (1:500; Cytoskeleton), followed by donkey anti-sheep IgG (H+L), Alexa Fluor 488 (1:500; Thermo Fisher Scientific) at 37°C for 1 h. It should be noted that methanol fixation could well preserve the continuous structure of MTs but cause loss of a fraction of soluble tubulins during fixation.

Turbidity assay

For turbidity assay, *in vitro* SUMOylation was performed in the 96-well microplate in a 100- μ l volume. The SUMOylated or control tubulins (–E2 or SUMO1 Δ GG) in the microplate were then supplemented with 1 mM GTP and incubated at 37°C for the polymerization measurement. Tubulin polymerization was monitored by recording the increase of turbidity as the absorbance at 350 nm (BioTek Synergy Neo Multi-Mode Microplate Reader) every 5 min for 2 h.

In vitro MT reconstitution assay

In vitro MT reconstitution assay was modified from a previous study (Gell et al., 2010). Briefly, the MT assembly and disassembly were carried out with a mixture of tubulin (SUMOylated or control) and Hilyte-488-conjugated GTP-tubulin (10:1) at 37°C in the BRB80 buffer supplemented with 25 mM glucose, 300 μ M glucose oxidase, 100 μ M catalase, 0.25 mg/ml bovine serum albumin, 50 mM KCl, 5 mM dithiothreitol, 0.1% methylcellulose, and 1 mM GTP. Tubulins were first SUMOylated and then used for MT reconstitution. The MT dynamics was observed with Hilyte-488-conjugated GTP-tubulin grown from the GMPCPP-stabilized MT seed labelled by rhodamine-conjugated tubulin. Images were collected every 5 sec for 20 min via TIRF microscope with Zeiss cell observer spinning disk system and a 100 \times oil lens. Images were converted to kymographs of MT dynamics with ImageJ. The typical events included MT growth and catastrophe at the plus end. The number of MT catastrophe was counted within 20 min to calculate the catastrophe frequency, and the average velocity of MT growth representing the growth rate and the longest distance of each MT during its growth episodes representing the maximum length were examined.

Protofilament formation assay, protofilament association assay, and imaging of protofilaments by negative-stain electron microscopy

Protofilament formation and association assays have been previously described (Portran et al., 2017). Briefly, protofilament formation was conducted by incubating 0.5 μ M SUMOylated or unSUMOylated tubulin in BRB80 with 1 mM GTP, 20 μ M Taxol (R&D, 1097), and 5% glycerol for 30 min at 4°C. The protofilaments were dialyzed in BRB80 containing 20 μ M Taxol for 1 h at 4°C using a D-tube Dialyser Mini (MWCO 6–8 kDa, Novagen) and 1 mM GDP was added after dialysis. Protofilament sheets were induced at 37°C for 30 min by adding 1 mM GDP. Finally, protofilaments and protofilament sheets were stained for observation by negative-stain electron microscopy. Formvar/carbon-coated grids (Zhongjingkeyi Technology) were treated with poly-L-lysine for 1 min, and protofilaments were added to grids for 1 min and then negatively stained with 1.5% uranyl acetate for 25–30 sec. Protofilaments and protofilament sheets were visualized using a FEI Tecnai G2 Spirit transmission electron microscope at 80 kV. The protofilament length and radius were measured using ImageJ by drawing a polyline on the protofilaments and fitting a circle from the polyline using the Fit Circle of ImageJ. The width of the protofilament sheets was measured using ImageJ and calculated as the protofilament number after dividing 4 nm (the width of a protofilament).

Analysis of MT plus end dynamics

HEK293 cells were seeded on 3.5-cm glass-bottom dishes, transfected with EB3-tdTomato and pCAG- α 1A-IRES-GFP or pCAG- α 1A(3KR)-IRES-GFP, and after 24 h imaged at a 0.5-sec

interval for 1 min with spinning disk confocal microscope (Andor Dragonfly) equipped with a $63\times/1.4$ NA oil objective and sCMOS (Zyla) or EMCCD (iXon Ultra 888) detectors at 37°C , 5% CO_2 . MT plus ends were automatically tracked using μ -Track software as previously described (Applegate et al., 2011; Movsisyan and Pardo, 2019) and growth rate and catastrophe frequency ($1/\text{mean}(T)$, where T is the lifetime of the growth subtrack just before catastrophe) were determined (Ertych et al., 2014).

Statistical analysis

Experiments were performed at least three times unless otherwise specified. The quantitative data were obtained from at least three independent experiments and shown as mean \pm SEM. Statistical significance was analyzed using two-tailed Student's t -test or Mann–Whitney test for two-group comparison using Prism 6 software (GraphPad). Differences were considered as significance at a level of $P < 0.05$.

Supplementary material

Supplementary material is available at *Journal of Molecular Cell Biology* online.

Acknowledgements

We thank Prof. Ying Jin for His-SUMO1 plasmid, Dr Didier Portran for the help with *in vitro* protofilament assays, and Dr Hao Sun for the help with SUMOylation detection. We thank the Core Facility for Cell Biology at Shanghai Institute of Biochemistry and Cell Biology and Integrated Laser Microscopy System at National Facility for Protein Science Shanghai, Zhangjiang Lab for technical assistance.

Funding

This work was supported by grants from the National Natural Science Foundation of China (31991194 and 31330046), the Strategic Priority Research Program of the Chinese Academy of Sciences (XDB19000000), and Shanghai Science and Technology Committee (18JC1420301).

Conflict of interest: none declared.

Author contributions: W.F. did most experiments in cells. R.L. did most of *in vitro* experiments. X.X. performed the PLA experiment. L.D. helped with *in vitro* experiments. N.G. helped with experiments in cells. Y.L. and X.Z. helped with the project design. J.C. provided *SENP1*^{+/-} mouse and plasmids. L.B., W.F., and R.L. wrote the manuscript. L.B. supervised the whole project.

References

Alonso, A., Greenlee, M., Matts, J., et al. (2015). Emerging roles of sumoylation in the regulation of actin, microtubules, intermediate filaments, and septins. *Cytoskeleton* 72, 305–339.

Applegate, K.T., Besson, S., Matov, A., et al. (2011). plusTipTracker: quantitative image analysis software for the measurement of microtubule dynamics. *J. Struct. Biol.* 176, 168–184.

Beauclair, G., Bridier-Nahmias, A., Zagury, J.F., et al. (2015). JASSA: a comprehensive tool for prediction of SUMOylation sites and SIMs. *Bioinformatics* 31, 3483–3491.

Becker, J., Barysch, S.V., Karaca, S., et al. (2013). Detecting endogenous SUMO targets in mammalian cells and tissues. *Nat. Struct. Mol. Biol.* 20, 525–531.

Castoldi, M., and Popov, A.V. (2003). Purification of brain tubulin through two cycles of polymerization-depolymerization in a high-molarity buffer. *Protein Expr. Purif.* 32, 83–88.

Chang, C.C., Tung, C.H., Chen, C.W., et al. (2018). SUMOgo: prediction of sumoylation sites on lysines by motif screening models and the effects of various post-translational modifications. *Sci. Rep.* 8, 15512.

Cheng, J., Kang, X., Zhang, S., et al. (2007). SUMO-specific protease 1 is essential for stabilization of HIF1 α during hypoxia. *Cell* 131, 584–595.

Conde, C., and Caceres, A. (2009). Microtubule assembly, organization and dynamics in axons and dendrites. *Nat. Rev. Neurosci.* 10, 319–332.

Dehmelt, L., Smart, F.M., Ozer, R.S., et al. (2003). The role of microtubule-associated protein 2c in the reorganization of microtubules and lamellipodia during neurite initiation. *J. Neurosci.* 23, 9479–9490.

Ertych, N., Stolz, A., Stenzinger, A., et al. (2014). Increased microtubule assembly rates influence chromosomal instability in colorectal cancer cells. *Nat. Cell Biol.* 16, 779–791.

Etienne-Manneville, S. (2013). Microtubules in cell migration. *Annu. Rev. Cell Dev. Biol.* 29, 471–499.

Geiss-Friedlander, R., and Melchior, F. (2007). Concepts in sumoylation: a decade on. *Nat. Rev. Mol. Cell Biol.* 8, 947–956.

Gell, C., Bormuth, V., Brouhard, G.J., et al. (2010). Microtubule dynamics reconstituted *in vitro* and imaged by single-molecule fluorescence microscopy. *Methods Cell Biol.* 95, 221–245.

Glotzer, M. (2009). The 3Ms of central spindle assembly: microtubules, motors and MAPs. *Nat. Rev. Mol. Cell Biol.* 10, 9–20.

Hendriks, I.A., D'Souza, R.C., Yang, B., et al. (2014). Uncovering global SUMOylation signaling networks in a site-specific manner. *Nat. Struct. Mol. Biol.* 21, 927–936.

Henley, J.M., Craig, T.J., and Wilkinson, K.A. (2014). Neuronal SUMOylation: mechanisms, physiology, and roles in neuronal dysfunction. *Physiol. Rev.* 94, 1249–1285.

Hofmann, W.A., Arduini, A., Nicol, S.M., et al. (2009). SUMOylation of nuclear actin. *J. Cell Biol.* 186, 193–200.

Impens, F., Radoshevich, L., Cossart, P., et al. (2014). Mapping of SUMO sites and analysis of SUMOylation changes induced by external stimuli. *Proc. Natl Acad. Sci. USA* 111, 12432–12437.

Janke, C. (2014). The tubulin code: molecular components, readout mechanisms, and functions. *J. Cell Biol.* 206, 461–472.

Janke, C., and Bulinski, J.C. (2011). Post-translational regulation of the microtubule cytoskeleton: mechanisms and functions. *Nat. Rev. Mol. Cell Biol.* 12, 773–786.

Kaminsky, R., Denison, C., Bening-Abu-Shach, U., et al. (2009). SUMO regulates the assembly and function of a cytoplasmic intermediate filament protein in *C. elegans*. *Dev. Cell* 17, 724–735.

Lee, C.C., Li, B., Yu, H., et al. (2018). Sumoylation promotes optimal APC/C activation and timely anaphase. *eLife* 7, e29539.

Letourneau, P.C., and Ressler, A.H. (1984). Inhibition of neurite initiation and growth by taxol. *J. Cell Biol.* 98, 1355–1362.

Lumpkin, R.J., Gu, H., Zhu, Y., et al. (2017). Site-specific identification and quantitation of endogenous SUMO modifications under native conditions. *Nat. Commun.* 8, 1171.

Magiera, M.M., Singh, P., Gadadhar, S., et al. (2018). Tubulin posttranslational modifications and emerging links to human disease. *Cell* 173, 1323–1327.

Manka, S.W., and Moores, C.A. (2018). The role of tubulin-tubulin lattice contacts in the mechanism of microtubule dynamic instability. *Nat. Struct. Mol. Biol.* 25, 607–615.

- Movsisyan, N., and Pardo, L.A. (2019). Measurement of microtubule dynamics by spinning disk microscopy in monopolar mitotic spindles. *J. Vis. Exp.* doi: 10.3791/60478.
- Nogales, E., Wolf, S.G., and Downing, K.H. (1998). Structure of the $\alpha\beta$ tubulin dimer by electron crystallography. *Nature* 391, 199–203.
- Panse, V.G., Hardeland, U., Werner, T., et al. (2004). A proteome-wide approach identifies sumoylated substrate proteins in yeast. *J. Biol. Chem.* 279, 41346–41351.
- Park, I.Y., Powell, R.T., Tripathi, D.N., et al. (2016). Dual chromatin and cytoskeletal remodeling by SETD2. *Cell* 166, 950–962.
- Pedrioli, P.G.A., Raught, B., Zhang, X.-D., et al. (2006). Automated identification of SUMOylation sites using mass spectrometry and SUMOOn pattern recognition software. *Nat. Methods* 3, 533–539.
- Portran, D., Schaedel, L., Xu, Z., et al. (2017). Tubulin acetylation protects long-lived microtubules against mechanical ageing. *Nat. Cell Biol.* 19, 391–398.
- Ren, J., Gao, X., Jin, C., et al. (2009). Systematic study of protein sumoylation: development of a site-specific predictor of SUMOsp 2.0. *Proteomics* 9, 3409–3412.
- Ribet, D., Boscaini, S., Cauvin, C., et al. (2017). SUMOylation of human septins is critical for septin filament bundling and cytokinesis. *J. Cell Biol.* 216, 4041–4052.
- Rodriguez, M.S., Dargemont, C., and Hay, R.T. (2001). SUMO-1 conjugation in vivo requires both a consensus modification motif and nuclear targeting. *J. Biol. Chem.* 276, 12654–12659.
- Rodriguez-Boulan, E., and Macara, I.G. (2014). Organization and execution of the epithelial polarity programme. *Nat. Rev. Mol. Cell Biol.* 15, 225–242.
- Rosas-Acosta, G., Russell, W.K., Deyrieux, A., et al. (2005). A universal strategy for proteomic studies of SUMO and other ubiquitin-like modifiers. *Mol. Cell. Proteomics* 4, 56–72.
- Sakakibara, A., Ando, R., Sapir, T., et al. (2013). Microtubule dynamics in neuronal morphogenesis. *Open Biol.* 3, 130061.
- Shea, T.B., Fischer, I., and Sapirstein, V.S. (1985). Effect of retinoic acid on growth and morphological differentiation of mouse NB2a neuroblastoma cells in culture. *Brain Res.* 353, 307–314.
- Snider, N.T., Weerasinghe, S.V., Iniguez-Lluhi, J.A., et al. (2011). Keratin hypersumoylation alters filament dynamics and is a marker for human liver disease and keratin mutation. *J. Biol. Chem.* 286, 2273–2284.
- Soderberg, O., Gullberg, M., Jarvius, M., et al. (2006). Direct observation of individual endogenous protein complexes in situ by proximity ligation. *Nat. Methods* 3, 995–1000.
- Song, Y., Kirkpatrick, L.L., Schilling, A.B., et al. (2013). Transglutaminase and polyamination of tubulin: posttranslational modification for stabilizing axonal microtubules. *Neuron* 78, 109–123.
- Stiess, M., and Bradke, F. (2011). Neuronal polarization: the cytoskeleton leads the way. *Dev. Neurobiol.* 71, 430–444.
- Tanaka, N., Meng, W., Nagae, S., et al. (2012). Nezha/CAMSAP3 and CAMSAP2 cooperate in epithelial-specific organization of noncentrosomal microtubules. *Proc. Natl Acad. Sci. USA* 109, 20029–20034.
- Tatham, M.H., Jaffray, E., Vaughan, O.A., et al. (2001). Polymeric chains of SUMO-2 and SUMO-3 are conjugated to protein substrates by SAE1/SAE2 and Ubc9. *J. Biol. Chem.* 276, 35368–35374.
- Ulrich, H.D. (2008). The fast-growing business of SUMO chains. *Mol. Cell* 32, 301–305.
- Vemu, A., Atherton, J., Spector, J.O., et al. (2016). Structure and dynamics of single-isoform recombinant neuronal human tubulin. *J. Biol. Chem.* 291, 12907–12915.
- Vethantham, V., and Manley, J.L. (2009). In vitro sumoylation of recombinant proteins and subsequent purification for use in enzymatic assays. *Cold Spring Harb. Protoc.* 2009, pdb.prot5121.
- Wang, Q., Peng, Z., Long, H., et al. (2019). Polyubiquitylation of α -tubulin at K304 is required for flagellar disassembly in *Chlamydomonas*. *J. Cell Sci.* 132, jcs229047.
- Witte, H., Neukirchen, D., and Bradke, F. (2008). Microtubule stabilization specifies initial neuronal polarization. *J. Cell Biol.* 180, 619–632.
- Wittmann, T., Hyman, A., and Desai, A. (2001). The spindle: a dynamic assembly of microtubules and motors. *Nat. Cell Biol.* 3, E28–E34.
- Zhang, R., Alushin, G.M., Brown, A., et al. (2015). Mechanistic origin of microtubule dynamic instability and its modulation by EB proteins. *Cell* 162, 849–859.
- Zhang, Y.Q., and Sarge, K.D. (2008). Sumoylation regulates lamin A function and is lost in lamin A mutants associated with familial cardiomyopathies. *J. Cell Biol.* 182, 35–39.
- Zhao, Q., Xie, Y., Zheng, Y., et al. (2014). GPS-SUMO: a tool for the prediction of sumoylation sites and SUMO-interaction motifs. *Nucleic Acids Res.* 42, W325–W330.
- Zhou, H.J., Xu, Z., Wang, Z., et al. (2018). SUMOylation of VEGFR2 regulates its intracellular trafficking and pathological angiogenesis. *Nat. Commun.* 9, 3303.